Comparison of an isotopic atmospheric general circulation model with new quasi-global satellite measurements of water vapor isotopologues

Kei Yoshimura,[1,2] Christian Frankenberg,[3] Jeonghoon Lee,[4] Masao Kanamitsu,[5] John Worden,[3] and Thomas Röckmann[6]

Received 29 March 2011; revised 19 July 2011; accepted 20 July 2011; published 14 October 2011.

[1] We performed an intensive comparison of an isotope-incorporated atmospheric general circulation model with vapor isotopologue ratio observation data by two quasi-global satellite sensors in preparation for data assimilation of water isotope ratios. A global Isotope-incorporated Global Spectral Model simulation nudged toward the reanalysis wind field, atmospheric total column data from Scanning Imaging Absorption Spectrometer for Atmospheric Cartography (SCIAMACHY) on Envisat, and midtropospheric (800 to 500 hPa) data from Tropospheric Emission Spectrometer (TES) on Aura were used. For the mean climatological δD of both the total atmospheric column and the midtroposphere layer, the model reproduced their geographical variabilities quite well. There is, however, some degree of underestimation of the latitudinal gradient (higher δD in the tropics and lower δD in midlatitudes) compared to the SCIAMACHY data, whereas there is generally less disagreement except lower δD over the Maritime Continent compared to the TES data. It was also found that the two satellite products have different relationships between water vapor amount and isotopic composition. Particularly, atmospheric column mean δD, which is dominated by lower-tropospheric vapor, closely follows the fractionation pattern of a typical Rayleigh-type "rain out" process, whereas in the midtroposphere the relationship between isotopic composition and vapor amount is affected by a "mixing" process. This feature is not reproduced by the model, where the relationships between δD and the vapor are similar to each other for the atmospheric column and midtroposphere. Comparing on a shorter time scale, it becomes clear that the data situation for future data assimilation for total column δD is most favorable for tropical and subtropical desert areas (i.e., Sahel, southern Africa, mideastern Asia, Gobi, Australia, and the southwest United States), whereas the available midtropospheric δD observations cover wider regions, particularly over tropical to subtropical oceans.

Citation: Yoshimura, K., C. Frankenberg, J. Lee, M. Kanamitsu, J. Worden, and T. Röckmann (2011), Comparison of an isotopic atmospheric general circulation model with new quasi-global satellite measurements of water vapor isotopologues, *J. Geophys. Res.*, *116*, D19118, doi:10.1029/2011JD016035.

1. Introduction

[2] Stable isotope ratio (δ^{18}O and δD) in water has been used not only as proxy information for paleoclimate reconstruction [*Dansgaard et al.*, 1969], but also as a natural tracer for hydrological cycles since the 1960s [*Dansgaard*, 1964]. Largely because of the isotope effects involved in phase changes of water, geographic and temporal variations of isotope ratios emerge in water vapor and precipitation. By using the isotope information in precipitation and vapor, one can study atmospheric vapor cycling processes on various scales, such as large-scale transport and in-cloud processes. Thus, the relationship between atmospheric processes and isotope information in water vapor and precipitation has been intensively studied [e.g., *Craig and Gordon*, 1965; *Ehhalt*, 1974; *Jouzel*, 1986; *Gedzelman and Arnold*, 1994; *Webster and Heymsfield*, 2003; *Yoshimura et al.*, 2003, 2004; *Worden et al.*, 2007].

[3] However, the very small amount of isotopic measurements compared to more "traditional" meteorological data (e.g., wind, water vapor, precipitation, and temperature) has greatly limited research. Though observations of precipitation isotopologues over land at time scales of a day to a

[1]Atmosphere and Ocean Research Institute, University of Tokyo, Kashiwa, Japan.
[2]Institute of Industrial Science, University of Tokyo, Tokyo, Japan.
[3]Jet Propulsion Laboratory, NASA, Pasadena, California, USA.
[4]Korea Polar Research Institute, Incheon, South Korea.
[5]Scripps Institution of Oceanography, University of California, San Diego, La Jolla, California, USA.
[6]Institute for Marine and Atmospheric Research Utrecht, Utrecht, Netherlands.

0148-0227/11/2011JD016035

month have been accumulated [e.g., *Welker*, 2000; *Kurita et al.*, 2004; *Bowen*, 2008], there are few precipitation isotope ratio observations over the ocean. Moreover, until recently observations of the isotope ratio of water vapor were severely lacking because traditional isotope measurement techniques are very complicated (e.g., the cryogenic method).

[4] Recent advances in remote sensing observations of water vapor isotopologue ratios via satellites have dramatically increased the number of observed data. *Zakharov et al.* [2004] retrieved the first latitudinal climatology for total column integrated water vapor δD values using the IMG (Interferometric Monitor for Greenhouse gases sensor) sensor on ADEOS. *Worden et al.* [2006] retrieved free tropospheric water vapor δD over tropical regions with fine temporal and spatial resolution using the Tropospheric Emission Spectrometer (TES) instrument on Aura. *Payne et al.* [2007] and *Steinwagner et al.* [2007, 2010] retrieved a global stratospheric δD distribution on a monthly basis using MIPAS (the Michelson Interferometer for Passive Atmospheric Sounding) on Envisat. *Frankenberg et al.* [2009] derived atmospheric total column δD values from Scanning Imaging Absorption Spectrometer for Atmospheric Chartography (SCIAMACHY) measurements on Envisat. Although limitations still exist in terms of spatial and temporal coverage, resolution, and accuracy, these observations have engendered greater understanding of the basic distribution of water isotopologues and the physical process that drives them. It is also worthwhile to mention that remote sensing with ground-based Fourier Transform Spectroscopy sensors has provided a useful and highly interesting new data set [e.g., *Schneider et al.*, 2010]. Furthermore, in the very recent past, precise optical analyzers for in situ HDO measurements have become available and will provide a wealth of information in the future [e.g., *Lee et al.*, 2006; *Welp et al.*, 2008].

[5] On the other hand, isotope-incorporated atmospheric general circulation models (AGCM) [*Joussaume et al.*, 1984; *Jouzel et al.*, 1987; *Hoffmann et al.*, 1998; *Mathieu et al.*, 2002; *Noone and Simmonds*, 2002; *Schmidt et al.*, 2005; *Lee et al.*, 2007; *Yoshimura et al.*, 2008; *Tindall et al.*, 2009; *Risi et al.*, 2010b; Y. Ishizaki et al., Interannual variability of $H_2^{18}O$ in precipitation over the Asian monsoon region, submitted to *Journal of Geophysical Research*, 2011] offer a different approach to understanding isotope ratio distribution. They combine the physical processes associated with isotope ratio changes with dynamic and moist thermodynamic processes of the atmosphere. These models simulate the time evolution of the three-dimensional structure of water vapor isotope ratio distribution with explicit consideration of complex water phase changes associated with moist physical processes in the global atmosphere. Most of the models' results generally match well with the precipitation isotope ratio observations for continental and monthly scales. For vapor isotope ratios however, the models are inconsistent [*Noone and Sturm*, 2010], and an intensive comparison with observations has not been made because of the lack of sufficient data except by *Schmidt et al.* [2005].

[6] As an advanced effort of the modeling approach, *Yoshimura et al.* [2008] (hereinafter Y08) ran an isotope-AGCM applying spectral nudging toward real atmospheric dynamics using the NCEP/DOE Reanalysis (R2) [*Kanamitsu et al.*, 2002] data set. This procedure mimics an isotope data assimilation, but without any observed isotope information. The global simulation forced by reanalysis better reproduced the isotope ratio variations in precipitation for a wide range of time scales from daily to interannual. This improvement by the nudging technique was confirmed by subsequent studies [e.g., *Risi et al.*, 2010b].

[7] In this paper, we validate various aspects of the Y08 isotope-AGCM historical simulation using newly published satellite δD products from SCIAMACHY [*Frankenberg et al.*, 2009] and TES [*Worden et al.*, 2007]. This is a further step toward potential data assimilation of water vapor isotope ratios and the production of objective analysis fields of isotope ratios, which have never yet been achieved. In section 2, the model simulation and the satellite-based products are described. Section 3 compares the results. A summary and conclusions follow.

2. Data and Method

2.1. SCIAMACHY δD Data

[8] In the work of *Frankenberg et al.* [2009], δD in the entire atmospheric column was measured for the first time by the SCIAMACHY grating spectrometer onboard the European research satellite Envisat. In a wavelength window ranging from 2355 to 2375 nm, simultaneous retrievals of HDO and H_2O vertical column densities are enabled. Because of the relatively high detector noise of SCIAMACHY in the short-wave infrared channel 8, the single measurement noise (1 sigma precision error) in δD is typically 40–100‰, depending on total water column, surface albedo and viewing geometry. This error can be significantly reduced by averaging multiple measurements, and the averaging procedure will be described below. The footprint of each measurement is 120 km by 30 km. The retrieval period for this study is 2003 through 2005, in which a total of about 1.9 million scenes are included and the measurement values of δD are systematically and arbitrarily decreased by 20‰ to minimize the large scale difference to the model and focus on the spatiotemporal variations only. More details about the retrieval procedure can be found in the work of *Frankenberg et al.* [2009]. Most noteworthy in regard to this study is the fact that SCIAMACHY measurements are performed in the short-wave infrared, thereby exhibiting sensitivity for the entire atmospheric column, including boundary layer water vapor.

2.2. TES δD Data

[9] TES on the Aura satellite is an infrared Fourier transform spectrometer that measures the spectral infrared (IR) radiances between 650 and 3050 cm^{-1} in limb-viewing and nadir (downward looking) modes. The observed IR radiance is imaged onto an array of 16 detectors that have a combined horizontal footprint of 5.3 km by 8.4 km in the nadir viewing mode. In the nadir view, TES estimates of atmospheric distributions provide vertical information of the more abundant tropospheric species such as H_2O, HDO, O_3, CO, and CH_4 [*Worden et al.*, 2006]. Simultaneous profiles of HDO and H_2O are obtained from TES thermal infrared radiances between 1200 and 1350 cm^{-1} (7400 to 8300 nm in wavelength) using maximum a posteriori optimal estimation [*Worden et al.*, 2006]. This approach allows for a precise

characterization of the errors in the ratio ([HDO]/[H_2O]) and its vertical resolution. For this analysis, mean values of the isotopologue ratio (δD) are calculated from averages of [HDO] and [H_2O] between 550 and 800 hPa, where the estimated profiles of δD are most sensitive. This average has a typical accuracy of 10‰ in the tropics and 24‰ at the poles. Profiles of atmospheric and surface temperature, surface emissivity, effective cloud optical depth and cloud top height are also estimated from TES radiances and are used to stratify δD analysis. A bias in the established HDO spectroscopic line strengths requires a special correction depending on its averaging kernel so that the degree of bias correction varies by each observation [*Worden et al.*, 2011]. The bias correction accounts for the a priori constraint and vertical resolution of the HDO and H_2O profile retrieval. In this study, the retrieval period is 2004 through 2008, in which a total of about 670,000 scenes are included, and the measurement values of δD are systematically and arbitrarily increased by 20‰ to minimize the difference to the model field over 45°S–45°N.

2.3. Common Shortcomings of Both the Satellite Data and Future Direction

[10] Here we should mention that neither TES nor SCIAMACHY are dedicated isotope instruments and that there exist systematic errors [*Worden et al.*, 2007; *Frankenberg et al.*, 2009]. For example, at higher latitudes (particularly poleward of 45°) the retrievals are very close to the a priori assumptions, which are likely erroneous. Furthermore, validations of these satellite products have been difficult because of lack of in situ measurements and difficulty in data handling. Therefore, the mismatches between the satellite measurements and the model, which are going to be discussed in the later parts of the paper, are not necessarily only due to model errors. As a first step in the improvement of both the satellite instruments and the model, however, it is necessary to reveal the agreement and disagreement between them and to understand their driving mechanism.

[11] For validating the satellite retrievals, there are some ongoing activities. A very recent paper by *Worden et al.* [2011] estimated the bias of TES by comparison to dedicated in situ measurements at Mauna Loa. *Schneider and Hase* [2011] reported on δD measurement by IASI (Infrared Atmospheric Sounding Interferometer) data with a higher temporal and spatial resolution than SCIAMACHY and TES, with measurement starting from 2007. Furthermore, the future TROPospheric Monitoring Instrument (TROPOMI) [*Levelt*, 2008] will provide HDO/H_2O retrievals in a manner similar to SCIAMACHY but with a greatly improved precision and temporal and spatial sampling frequency. Similar algorithm of SCIAMACHY is applicable to a Fourier Transform Spectrometer (FTS) on the Japanese CO_2 monitoring satellite Greenhouse gases Observing SATellite (GOSAT) (C. Frankenberg, private communication, 2010). In addition, there is the recently started project MUSICA (Multiplatform remote Sensing of Isotopologues for investigating the Cycle of Atmospheric water, http://www.imkasf.kit.edu/english/musica). It aims on a consistent on a consistent δD data set applying ground- and space-based remote sensing as well as surface and aircraft in situ measurement techniques.

2.4. Isotope General Circulation Model Simulation

[12] The Isotope-incorporated Global Spectral Model (IsoGSM) was developed by Y08 and a 30 year simulation with a global spectral nudging technique [*Yoshimura and Kanamitsu*, 2008] was performed (data available at http://hydro.iis.u-tokyo.ac.jp/~kei/IsoGSM1). The spatial and temporal resolution of the IsoGSM simulation atmospheric output is 2.5° × 2.5° and 6 hourly. In this study, this nudged simulation data is used for comparisons with the satellite measurements. In this method, the large-scale dynamical forcing was taken from NCEP/DOE Reanalysis 2 [*Kanamitsu et al.*, 2002], and water isotope ratios were fully predicted, including their sources and sinks, without utilizing any water isotope observations. Several validation studies of this model product against limited observations showed that the analysis is sufficiently accurate for various process studies [e.g., *Uemura et al.*, 2008; *Abe et al.*, 2009; *Schneider et al.*, 2010; *Berkelhammer et al.*, 2011].

[13] We prepare a further experiment to examine the sensitivity of the results to the “equilibrium fraction ε,” which is the degree to which falling raindroplet equilibrates with the surroundings. This parameter is very important to the isotopic exchange between falling droplet and ambient vapor [*Hoffmann et al.*, 1998; *Lee and Fung*, 2008; *Yoshimura et al.*, 2010]. It is the essential reason precipitation isotope ratios only reflect the near surface vapor even though the condensation takes place at a much higher atmospheric level. The experiment using the smaller equilibrium fraction of 10% for convective precipitation is called E10 hereafter, whereas the control run (CTL) used an equilibrium fraction of 45%. This decrease of the parameter indicates that a raindrop in a convective cell would less isotopically interact with the ambient vapor than previously thought. The simulation period of E10 with the same nudging scheme starts from 2000, so that the impact of the initial state is sufficiently dissolved for the analysis period of 2003–2007.

[14] With a similar purpose, *Lee et al.* [2009] conducted sensitivity tests to quantify the impact of the time scale for consumption of convective available potential energy (CAPE) on the isotopic distribution. We chose a different way to change a parameter which influences the stable water isotope ratios only similar to the work of *Lee and Fung* [2008] and *Field et al.* [2010], since we want rather not to modify the convective process itself, since the convective process has been long tested, and moreover, it influences the general circulation itself.

2.5. Processing of the Data

[15] From the IsoGSM simulation results, the nearest location and time of each satellite measurement are extracted for both SCIAMACHY and TES data (hereafter the process is called “collocation”). Thus there is no representativeness difference between the model and the data. The extraction process for SCIAMACHY data is different from that for TES. Since a single measurement by SCIAMACHY has a larger random error [*Frankenberg et al.*, 2009], we average multiple measurements that have been collected for a grid of 2.5° × 2.5° in 6 h, whereas no averaging of multiple measurements is taken into account for the TES-IsoGSM collocation. We set the threshold value for the averaging as 10. Therefore, the average of the SCIAMACHY

measurements is only considered for comparison with IsoGSM if the measurements were made more than 10 times inside a cell of 2.5° × 2.5° for 6 h. After this procedure, the amount of comparable data shrinks to about 50,000, mainly covering the desert regions because of the high IR reflectivity and absence of clouds there [*Frankenberg et al.*, 2009].

[16] Because there is some degree of vertical sensitivity regarding the averaging kernels (AK) of the satellite sensors' retrieval algorithms particularly apparently for the TES data, we have applied the AK for each collocated data for TES and calculated the mean δD values for 800–500 hPa level, whereas we have simply extracted the mean δD values in the vapor contents of the total atmospheric column for SCIAMACHY. The application of the TES AK suggested by *Lee et al.* [2011] is written as follows:

$$\mathbf{X}_{GCM}^{New} = \mathbf{X}_a + \mathbf{A}_{TES}[\mathbf{X}_{GCM} - \mathbf{X}_a]$$

$$\mathbf{X} = \begin{bmatrix} \ln(q_{D(1)}) \\ \vdots \\ \ln(q_{D(25)}) \\ \ln(q_{H(1)}) \\ \vdots \\ \ln(q_{H(25)}) \end{bmatrix} \quad \mathbf{A}_{TES} = \begin{bmatrix} \mathbf{A}_{DD} & \mathbf{A}_{DH} \\ \mathbf{A}_{HD} & \mathbf{A}_{HH} \end{bmatrix}$$

where $q_{D(k)}$ and $q_{H(k)}$ are volume mixing ratio of HDO and H_2O, respectively, at TES vertical level k up to 25th level (100 hPa), and suffixes of a and GCM indicate a priori assumption and IsoGSM result, respectively. A_{TES} is the averaging kernel matrix of TES.

[17] The TES's AK vary in time and space and TES is less sensitive where there is little water vapor, such as at high latitudes. With the low sensitivity, the retrieval results tend to be close to the a priori assumption, which is why TES sees a smaller latitudinal gradient and smaller seasonal cycles at high latitudes [*Worden et al.*, 2006]. On the other hand, SCIAMACHY's AK do not vary in time and space. It should be noted that this study first applied TES AK at each single observation occurrence, whereas the previous studies did for time averages such as monthly climatology [*Lee et al.*, 2011; C. Risi et al., Process evaluation of tropical and subtropical tropospheric humidity simulated by general circulation models using water vapor isotopic observations, submitted to *Journal of Geophysical Research*, 2011]. Thus, the use of the nudged simulation is essential for this study.

3. Results

3.1. Comparison of Annual and Seasonal Climatology

[18] In Figure 1, the annual mean climatology of the SCIAMACHY measurement (Figure 1a) and the collocated IsoGSM simulations (Figures 1b and 1d) are shown. IsoGSM is a state-of-the art model that captures the general two-dimensional isotopic distribution well. The common maxima over central Africa and the Amazon are likely due to the impact of evapotranspiration from the land surface, leading to isotope enrichment. Over these regions, the "continental effect" is weaker than over midlatitudes and high latitudes as shown by *Frankenberg et al.* [2009]. It is important to note that the annual averages shown in Figure 1 are biased toward specific seasons because the observation frequency depends on many factors, such as minimum signal-to-noise ratio, cloud cover, or thresholds on solar zenith angles (resulting in less measurement at high latitudes where snow cover and high solar angles reduce the signal level in the short-wave infrared). Whereas this must be taken into account when interpreting the data, it does not affect the model-data comparison because of the collocation.

[19] Despite the qualitatively good agreement, there are also some discrepancies, and the most obvious difference is that the simulated latitudinal isotope gradient is smaller than in the observations. These differences between the model and SCIAMACHY observations are shown in Figure 1c and 1e and they reveal that compared to SCIAMACHY, both experiments in IsoGSM underestimate the tropical δD values whereas they overestimate subtropical δD. The difference between the two experiments (Figure 1b and 1d) is relatively smaller, indicating that the impact of the equilibrium fraction factor ε is not as sensitive at the atmospheric column as at the middle troposphere (will be shown in Figure 2).

[20] In Figure 2, the geographical comparisons between the TES data and the collocated and AK-applied IsoGSM results are shown in a similar manner. As for the SCIAMACHY results, the spatial pattern is qualitatively well simulated by both experiments (Figures 2a, 2b, and 2d). Without application of AK, the model overestimates the latitudinal gradient (figure not shown), but such overestimation is corrected by AK application. This might be partly because the TES sensitivity declines at increasing latitudes so that the retrieved values become closer to the a priori, in turn damping both the seasonality and the latitudinal gradients. Moreover, there are large underestimations over the Maritime Continent and Central America as illustrated in Figure 2c, where convective precipitation is most significant. The reason for this big discrepancy will be discussed below.

[21] In Figures 2d and 2e, we compare the E10 results with the satellite retrievals. The impact of changing the equilibrium fraction is apparent over the Maritime region where the discrepancy in the control run was large. The large change in the midtropospheric vapor δD is compensated by the changes in precipitation (figure not shown) and surface vapor δD (difference between Figures 1b and 1d) due to the mass balance, but the compensated changes are smaller because of the larger amount of water at near surface or in precipitation than at midtroposphere. This result is consistent with what *Field et al.* [2010] obtained in their model.

[22] Figure 3 illustrates zonal and tropical averages of SCIAMACHY and IsoGSM data for annual, June, July, and August (JJA) and December, January, and February (DJF) climatology. The zonal averages (Figures 3a to 3c) again highlight the model's underestimation of the latitudinal gradient in vapor δD (less enrichment at the tropics and over-enrichment elsewhere). The tropical underestimation is largest in the DJF season. More detailed information about the origin of the mismatch in the tropics can be obtained by examining the longitudinal variations in the 30°S to 30°N latitudinal belt as illustrated in Figures 3d to 3f. The model's underestimation is larger in the eastern half of the tropics (Figure 3d). The JJA longitudinal variation (Figure 3e) is reasonably reproduced by the model, but the model misses the significant enrichment in the 20°W to 20°E region, which corresponds to the tropical African region (around

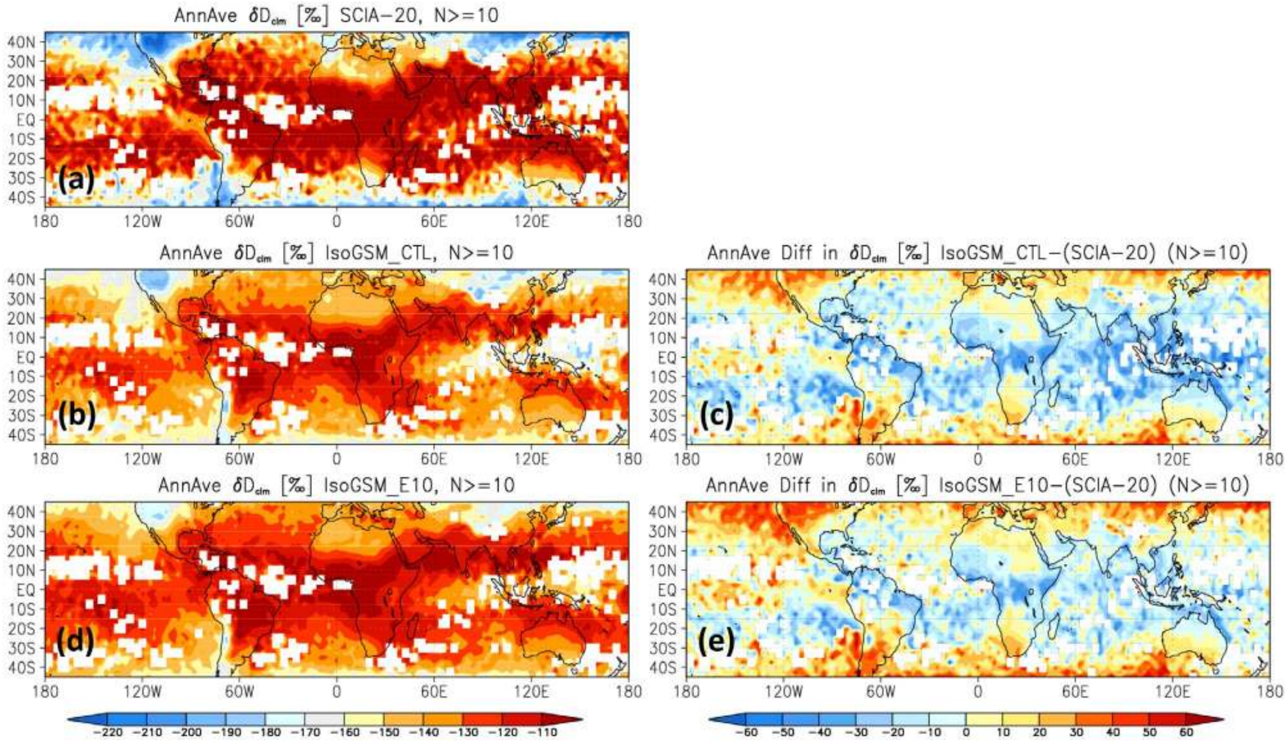

Figure 1. (left) Annual mean climatology of δD in atmospheric vapor for (a) Scanning Imaging Absorption Spectrometer for Atmospheric Cartography (SCIAMACHY), (b) collocated Isotope-incorporated Global Spectral Model (IsoGSM) control run (CTL) experiment, and (d) collocated IsoGSM experiment using the smaller equilibrium fraction of 10% for convective precipitation (E10). (right) Differences between the satellite measurements and model simulations for (c) CTL and (e) E10. SCIAMACHY δD data is systematically decreased by 20‰.

10°S–10°N). This implies that the model misses an important process of isotope enrichment in this region, if the SCHIAMACHY data is trustable enough. Though it is rather wet region, more intensive vapor recycling process [e.g., *Numaguti*, 1999] would have been taken into account than the model simulates. The DJF tropical zonal variation (Figure 3f) is poorly simulated, and discrepancy between the model and the satellite seems larger in the eastern half of the tropical band. This larger discrepancy for δD strongly contributes to the annual average over the eastern half. The sensitivity run E10 consistently increased the δD of vapor because of the reduced isotopic exchange between falling droplets and ambient vapor. The global average of the increase was about 6‰, and slightly larger at the tropics. Nevertheless, the strong longitudinal variability of the measurements in the winter months is still not captured by the model.

[23] Figure 4 is similar to Figure 3, but for the TES data. Furthermore, IsoGSM results without AK application are also shown. Without AK, the model-data difference becomes particularly large poleward of 45°, where TES's degrees of freedom for the retrieval of the δD is substantially smaller than 1 [*Worden et al.*, 2006]. With AK, this difference is dramatically resolved. However, because of the erroneous feature at high latitudes mentioned before, we do not further interpret the high-latitude data. Equatorward of 45°, however, the model's latitudinal gradient matches the observations reasonably well both with and without AK application. For the tropical longitudinal variations (Figures 4d to 4f), the model follows the large-scale patterns much better than for the SCIAMACHY data. In general, the model overestimates the depletion between 100°E and 180° which corresponds to the Maritime Continent and surrounding oceans. This feature was previously noted in the description of Figure 2c. The amplification of the strong depletion is reduced for DJF (Figure 4f), and the overall match becomes better than that of JJA. As a result of averaging over the entire year, the annual latitudinal variation of CTL is slightly overamplified in the model (Figure 4d). However, this erroneous feature is partly fixed by the E10 experiment, particularly over the Maritime Continent and surrounding oceans at JJA. The smaller equilibrium fraction increased the δD of midtropospheric vapor by up to 30‰, a much larger amount than that of the total atmospheric column vapor as previously noted.

[24] In Figure 5, scatter diagrams between the satellites' observation climatologies and the IsoGSM simulation climatology are shown. This time only the E10 result is shown because of the better match toward the satellite data. Figures 5a to 5c shows that the distribution pattern is reasonably well simulated with a correlation coefficient (R) of $0.78 \sim 0.81$. As discussed above, the range of the IsoGSM's spatial and temporal distribution in atmospheric column δD is smaller than that of SCIAMACHY by a factor of $0.49 \sim 0.50$ (i.e., $\sigma_{\mathrm{sim}}/\sigma_{\mathrm{obs}}$). On the contrary, the midtropospheric δD is simulated with a slightly larger variance for spatial distribution

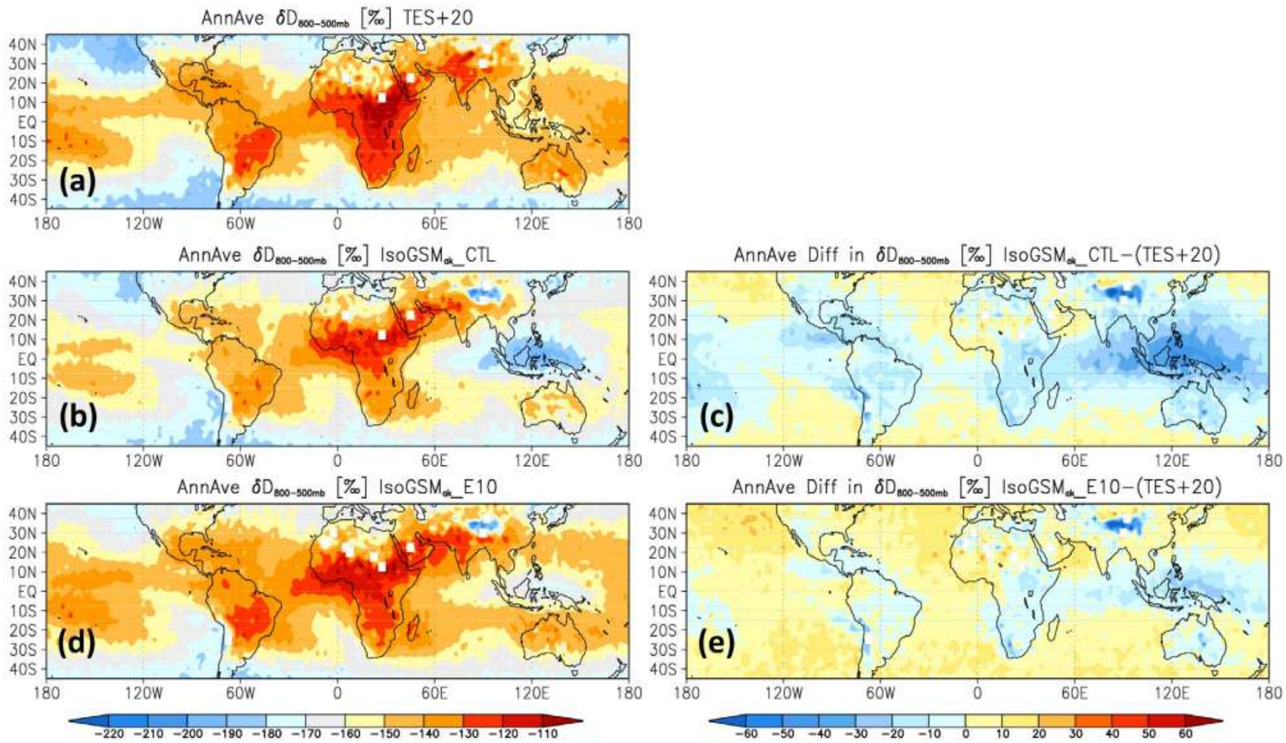

Figure 2. Same as Figure 1 but for Tropospheric Emission Spectrometer (TES) midtropospheric (800 to 500 hPa pressure) observation. TES δD data is systematically increased by 20‰. TES's averaging kernel is applied to each collocated IsoGSM data.

compared to the TES observation, by a factor of 0.83 ~ 0.94 with a correlation coefficient of 0.76 ~ 0.84, as shown in Figures 5d to 5f. It should be noted that the distinctive area of the larger discrepancy in the TES comparison is still visible, particularly in Figure 5e. This is derived from the model's underestimation of δD over the Maritime Continent and Central America compared to TES, as mentioned above, whereas the discrepancy was much larger in the CTL experiment.

[25] The general comparisons of correlation coefficients and slopes between the model simulations and the data are

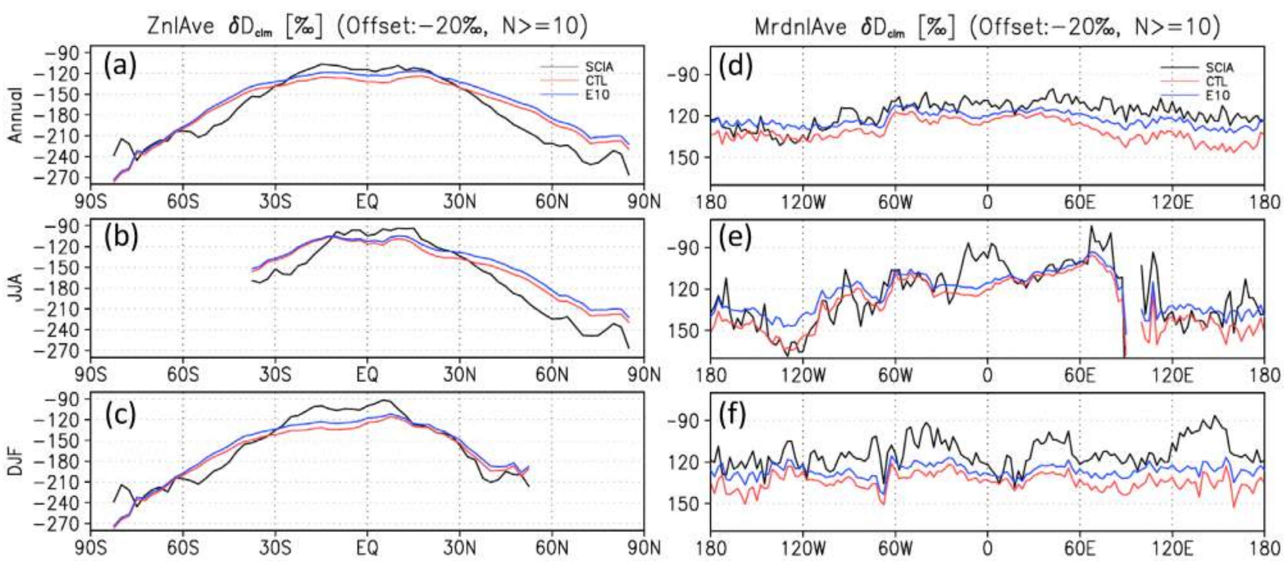

Figure 3. (a–c) Zonal and (d–f) meridional averages of modeled (CTL is red and E10 is blue) and observed (black) δD in atmospheric column vapor by SCIAMACHY. The zonal averages (Figures 3a to 3c) are for all longitudes, whereas the meridional averages are for the tropical regions (equatorward of 30°). Figures 3a and 3d represent annual climatology, Figures 3b and 3e are for June, July, and August (JJA) means, and Figures 3c and 3f are for December, January, and February (DJF) means.

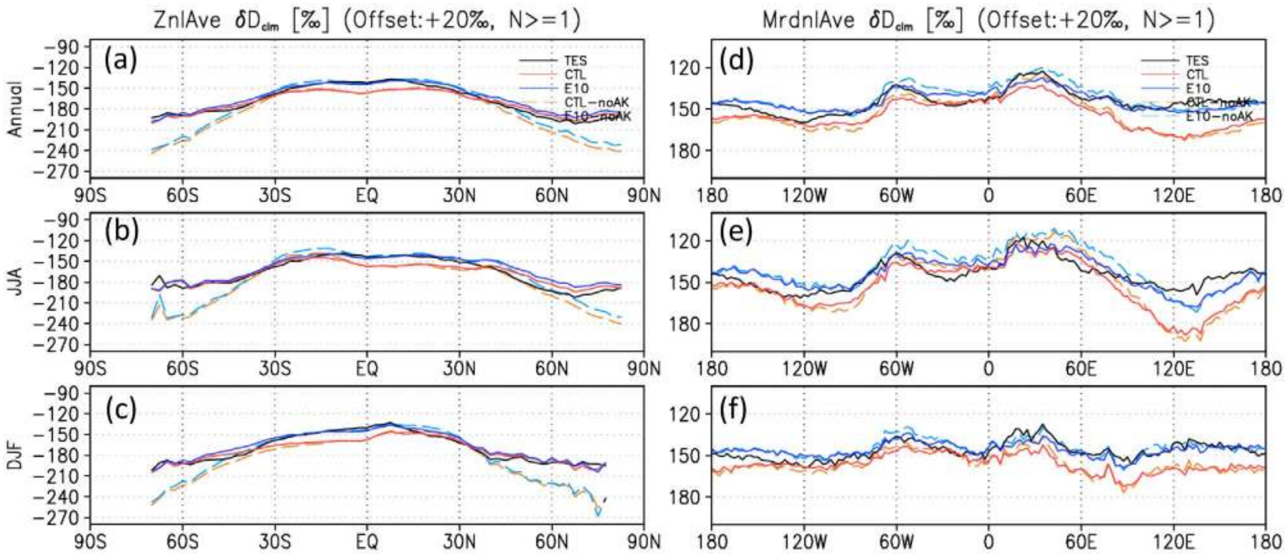

Figure 4. Similar to Figure 3 but for the TES midtropospheric δD. For reference, the IsoGSM results without TES's averaging kernel ("noak") are shown by orange and sky blue dashed lines for CTL and E10 experiments, respectively.

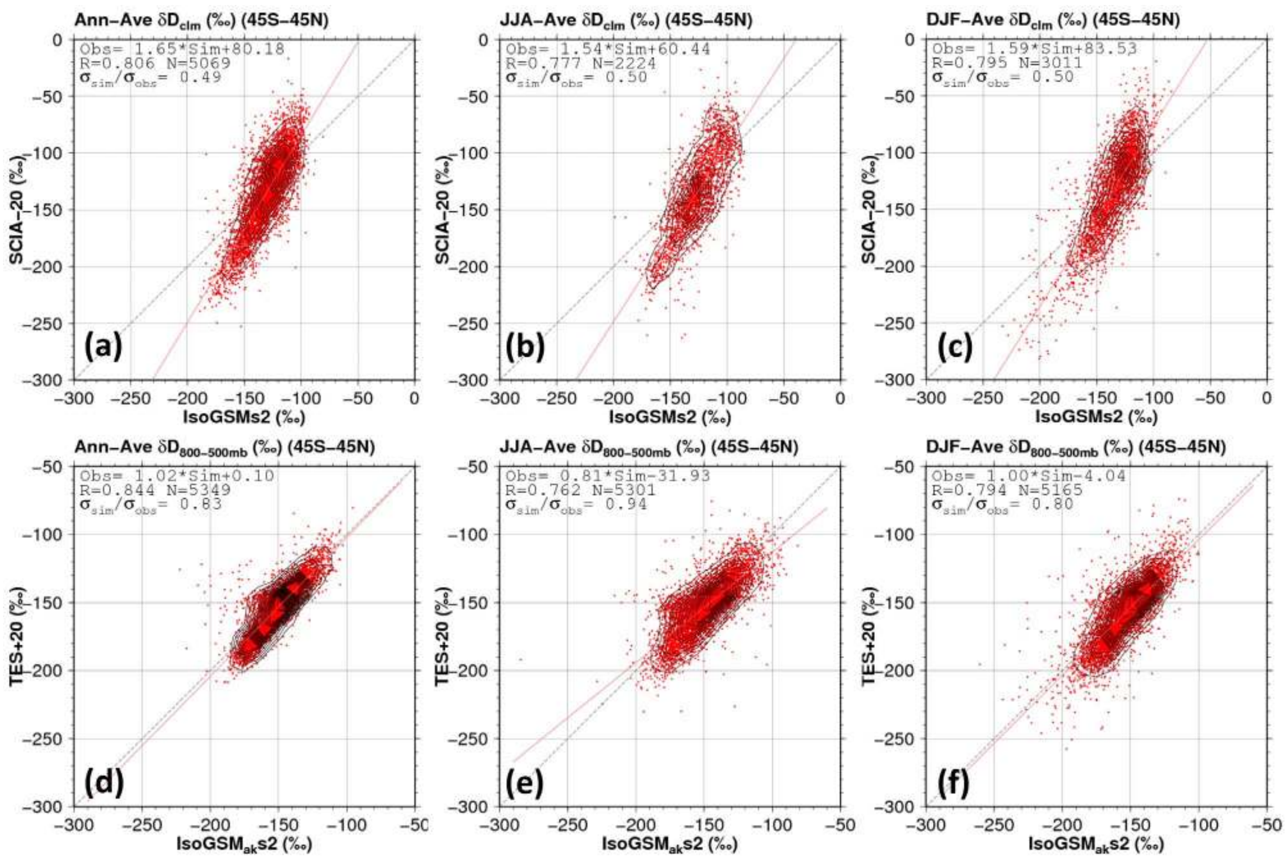

Figure 5. Scatter diagrams between the satellites' observations and the IsoGSM E10 simulation climatology covering 45°S–45°N. (a–c) SCIAMACHY data and (d–f) TES data. Figures 5a and 5d are for annual average, Figures 5b and 5e are for JJA, and Figures 5c and 5f are for DJF. Contours indicate relative frequency of the two-dimensional histograms with a contour interval of 0.5% and a class range of 10‰ for each axis.

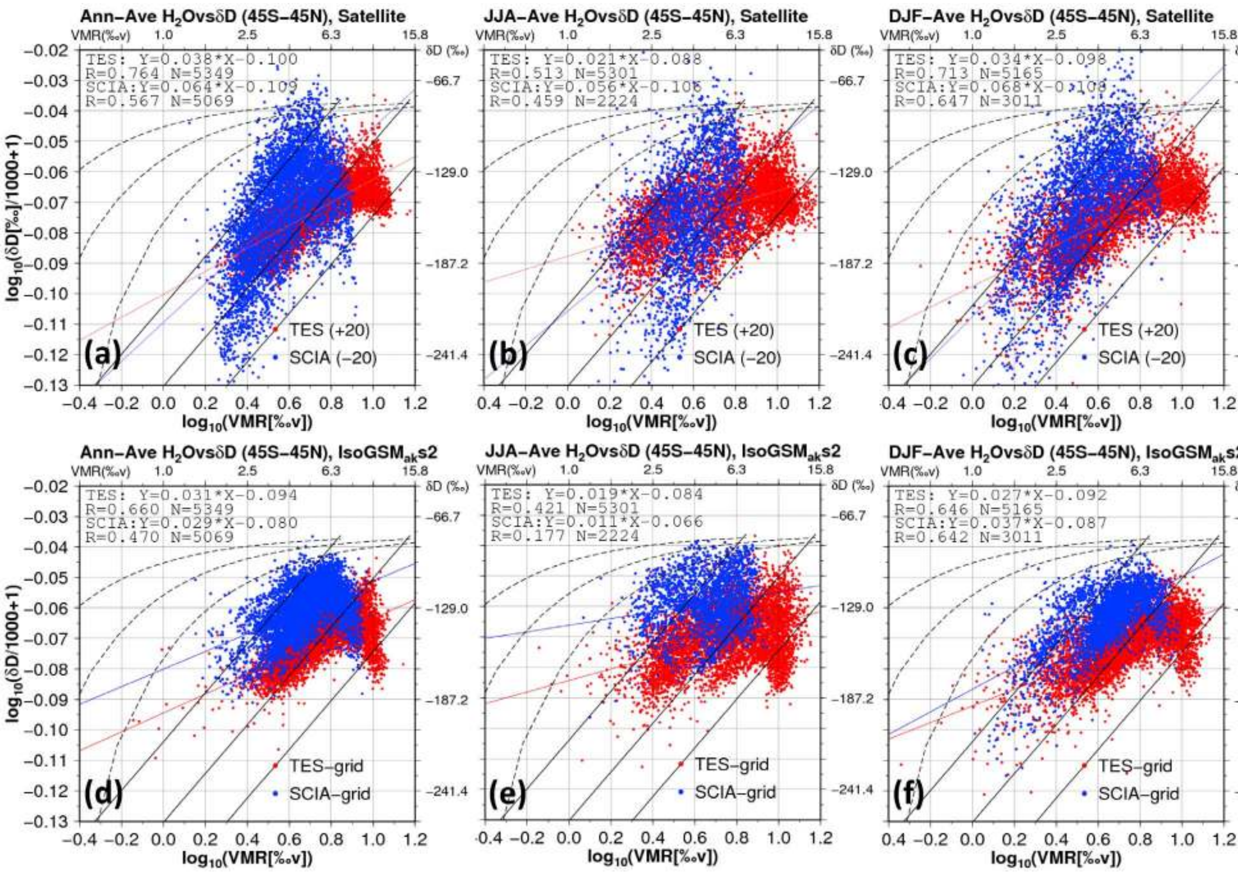

Figure 6. Scatter diagrams between vapor δD and humidity in bilogarithm expression. (a–c) Satellite observation climatology and (d–f) IsoGSM E10 simulation climatology. Blue and red dots represent SCIAMACHY and TES observations (or collocations), respectively. Figures 6a and 6d are for annual average, Figures 6b and 6e are for JJA, and Figures 6c and 6f are for DJF. The black solid lines indicate the Rayleigh-type fractionation, where heavy isotopes are preferably removed from vapor by condensation, starting from three typical vapors originating from the sea with 5°C, 15°C, and 25°C. The black dashed lines indicate so-called "mixing lines," which represent the mixing of two isotopically distinctive air masses (−350‰ and −80‰) starting with three different vapor amount (VMR) of 0.07 0.15 0.30‰v) for the depleted air mass.

not very time sensitive. Figures 5b and 5c show the relationships for JJA and DJF, respectively, for total atmospheric column δD with SCIAMACHY data, and Figures 5e and 5f show the same for midtropospheric δD with TES data. The area of the biggest discrepancy between TES and IsoGSM is more apparent in JJA than DJF, which is probably due to the more active convective precipitation over the mismatched regions in summer.

3.2. Relationship Between Vapor Amount and δD

[26] Figure 6 presents relationships between water vapor amount (volume mixing ratio or VMR in ‰v) and its δD in the satellite observations and the simulation over tropical to midlatitudinal regions (45°S to 45°N). Both axes are in logarithm representation; i.e., the vertical axis is log(δD + 1), and the horizontal axis is log of VMR, so that a typical Rayleigh distillation process should form a straight line whose slope equals the fractionation factor α minus 1. Figures 6a to 6c, in which both the SCIAMACHY (blue dots) and TES observations (red dots) are plotted, indicates that the slopes of the linear regressions in SCIAMACHY are steeper than those of TES. However, these slopes (0.056 ~ 0.068 for SCIAMACHY and 0.021 ~ 0.038 for TES) are all smaller than that of a typical Rayleigh distillation process line (black solid lines), which should be around 0.08 ~ 0.15 depending on ambient temperature (+20 ~ −20C) [*Majoube*, 1971a, 1971b]. This difference is partly caused by the omission of high-latitude regions in both observational data sets, where typically Rayleigh processes dominantly affect the variation of δD. More importantly, the distinct differences between the SCIAMACHY and TES plots imply that surface vapor is more influenced by the Rayleigh-type rainout process, whereas the midtroposphere vapor is more influenced by mixing of isotopically distinct vapor masses without isotope fractionation. This implication agrees with the previous finding [*Galewsky and Hurley*, 2010]. Furthermore, there is a negative correlation in the TES plots where VMR is larger than 10‰v. This is due to the "amount effect" [*Dansgaard*, 1964; *Lawrence et al.*, 2004; *Lee and Fung*, 2008; *Risi et al.*, 2008; *Field et al.*, 2010] over the tropics, where much rain and its vapor are associated with some heavy isotope depletion.

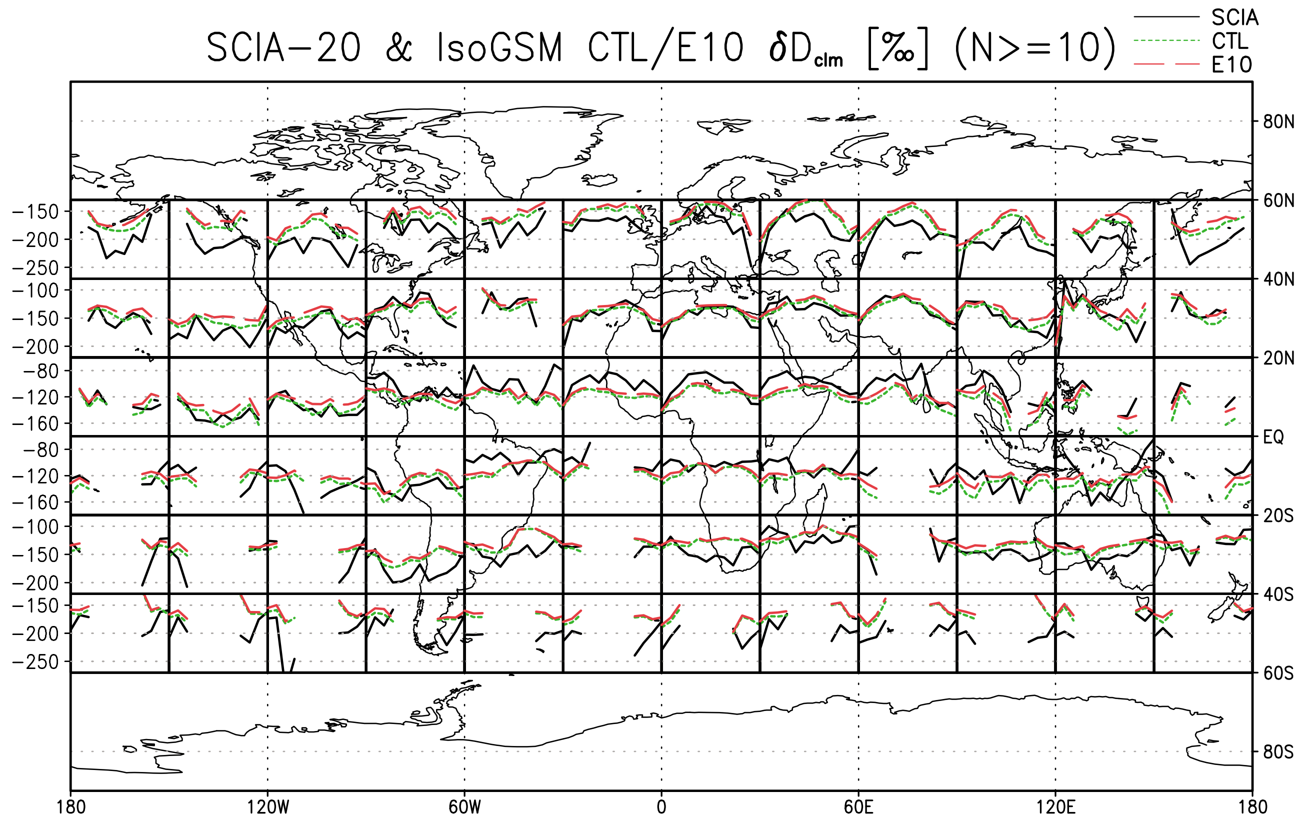

Figure 7. Global distribution of δD seasonal variations using SCIAMACHY data (black lines) and two IsoGSM simulations (green dotted lines for CTL and red dashed lines for E10).

[27] In the model (Figures 6d to 6f), these relationships are differently simulated. First, the negative correlations at high vapor amounts are much more apparent than in the measurements. This feature is particularly distinguishable over the Maritime Continents and it is arguably stated that the amount effect associated with convective process is to some extent overestimated in the model. Second, the slopes of the linear regression lines for atmospheric column vapor (0.011 ~ 0.037) became similar to those for midtroposphere (0.019 ~ 0.031), whereas the satellite observations showed the steeper slopes for SCIAMACHY than TES. Third, these simulated values for the SCIAMACHY observation have much shallower slopes than the observation, whereas both of the slopes are more similar for TES.

[28] Such an analysis of the slope (α-1) has been discussed by *Schneider et al.* [2010] at two ground sites. In their results [*Schneider et al.*, 2010, Figure 7], the slope is higher at surface and decreased with height. This relationship is consistent in the TES/SCIAMACHY comparison, even though their analysis is based on temporal variability whereas ours is on spatial variability. The consistent results are obtained in the model too, i.e., the slope tends to stay unchanged (at subtropics) or slightly increased (at subarctic).

3.3. Seasonal Variations in Vapor δD

[29] Figures 7 and 8 show 3 year averaged annual cycles of regional means over 30° × 20° (longitude × latitude) regions for SCIAMACHY and TES, respectively. To make the monthly averaged regional means, simple arithmetic averages of all monthly 2.5° × 2.5° data over a 30° × 20° region were used. The respective collocated simulation results of both CTL (green dotted lines) and E10 (red dashed lines) are also shown. In general, the seasonal variations of both satellite data sets are well reproduced by the simulations in most regions.

[30] In comparing the SCIAMACHY and IsoGSM simulations (Figure 7), remarkable consistency is observable over the 20°N–40°N latitude band. Because of the weaker latitudinal gradient in the model simulation, there are overestimation biases at higher latitudes (>40°N) and underestimation bias at lower latitudes (<20°N). However, the patterns of the seasonal variations are reasonably well reproduced over the Northern Hemisphere in both experiments. In the Southern Hemisphere, however, the reproducibility is not as good. This is partly because the skill of the IsoGSM atmospheric analysis over the SH is not as good as over the NH (Y08). Also, the SCIAMACHY measurements have less credibility over oceans [*Frankenberg et al.*, 2009].

[31] The seasonal variations observed by TES are also reasonably reproduced by IsoGSM over low to middle latitudes (40°S to 40°N), except over the Maritime Continents (20°S–20°N and 90°E–180°) by CTL. As mentioned above, the discrepancy over the Maritime Continents is likely derived from the poor representation of isotopic behavior in convective processes, particularly related to the isotopic exchange process between falling droplets and ambient vapor. E10 shows much better seasonal variation over these regions.

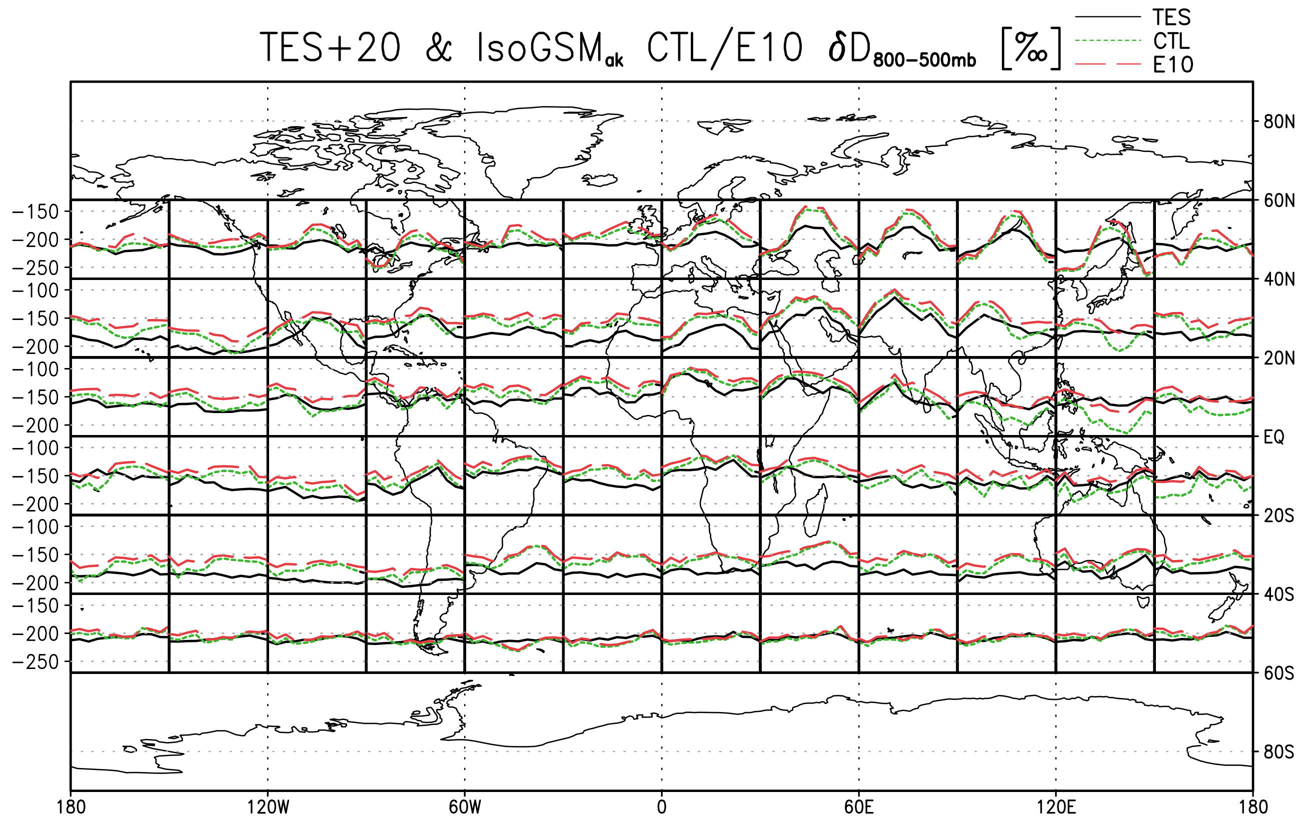

Figure 8. Same as Figure 7 but for TES midtropospheric data.

3.4. Comparison in Short-Term Temporal Variations

[32] In Figure 9, the time series of atmospheric column mean δD and TPW (total precipitable water) from SCIAMACHY and the IsoGSM E10 experiment at a specific grid point of 15°E and 20°N (Sahel region) for the year of 2005 are shown. Since the basic feature is almost the same, the CTL experiment is omitted. As already noted, a single gridded data point from SCIAMACHY is an average of more than 10 single measurements in a 2.5° × 2.5° and 6 h space. Single measurements by SCIAMACHY fluctuate greatly, particularly for δD, as shown by small dots in Figure 9. However, despite the large range of the fluctuation, the spatiotemporal averages for the vapor δD are reasonably well reproduced by the model (R = 0.749). Note that this correlation is calculated using the averaged data for observation, therefore the random noise by single measurement hardly affected the result. Although it may be necessary to more carefully investigate the systematic and representativeness error characteristics, the good match in variability and sufficient number of valid measurements (N = 64) point to promising potential for four-dimensional data assimilation in the future.

[33] Compared to the isotope information, the TPW from the model and measurements match much better (R = 0.882), with smaller fluctuations from each data set. Though related via Rayleigh processes, the isotopic composition has independent variability from that of water vapor amount. Consequently the assimilation of the isotope information would give some additional constraint to the model, which may affect the quality of the hydrological cycle and forecasting predictability.

[34] *Risi et al.* [2010a] show a similar plot at Niamey (13.52°N, 2.09°E) in there Figure 4. They pointed out that the model significantly underestimated the short-term peak-to-peak fluctuations compared to SCIAMACHY. This is somewhat true in this study, too, as the slope of the regression line is 1.54 (Figure 9b), but it seems the IsoGSM shows closer agreement to the satellite data in terms of the amplitudes of short-term variability.

[35] Figure 10 shows similar plots to Figure 9, but for TES at 67.5°E and 25°N (over the Arabian Sea) for 2006. δD (Figure 10a and 10b) and volume mixing ratio of water vapor (Figure 10c and 10d) of mean middle (800 hPa to 500 hPa) tropospheric air are shown. The 6 hourly model simulation without AK application is shown as reference, too (sky blue lines). Unlike the SCIAMACHY case, there is no spatiotemporal averaging, so that each red dot in Figure 10 represents a single measurement by TES. Though the correlation coefficient is smaller than that of Figure 9 for a SCIAMACHY time series, it is a positive correlation between observed and modeled midtropospheric δD (R = 0.681). The amplitude of model variability is slightly larger than that of TES (slope = 0.61) even though the TES data does not have any averaging in a grid. This means that compared to the model the TES observations appear to miss some extent of the short-term variability, which could be a limitation when data assimilation is considered. The volume mixing ratio shows higher reproducibility than δD, similar to SCIAMACHY.

[36] Figure 11 shows two-dimensional maps of correlation coefficients obtained from the comparison of high-frequency seasonal variations as in Figures 9 and 10 between SCIAMACHY and the IsoGSM E10 model run

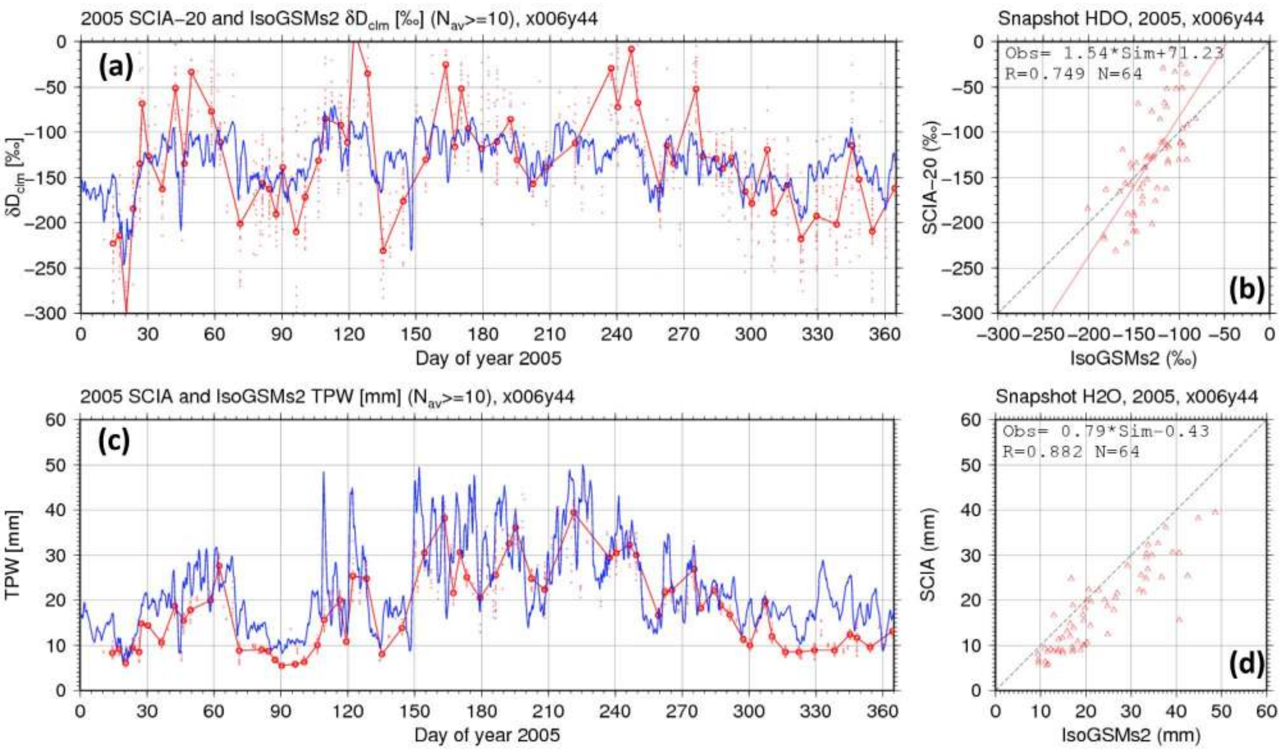

Figure 9. Comparison of the snapshot measurements with the simulation at a grid of 15°E and 20°N. (a and b) δD of atmospheric column vapor and (c and d) the amount of total precipitable water (TPW). Time series are on the left (Figures 9a and 9c), and scatterplots are on the right (Figures 9b and 9d). In Figures 9a and 9c, red circles and blue lines represent SCIAMACHY and the IsoGSM E10 simulation, respectively, while the small red dots are from SCIAMACHY single measurements before averaging for 6 h and 2.5° × 2.5° space.

(Figure 11a and 11b), and between TES and IsoGSM E10 (Figure 11c and 11d). From the SCIAMACHY figures, it is shown that a valid grid with more than 10 comparable data during 2005 is preferably located in the tropical and subtropical desert areas (i.e., Sahel, southern Africa, middle east Asia, Gobi, Australia, and southwest United States). The temporal variability of atmospheric column δD is reasonably reproduced ($R > 0.6$) by the model in these areas (Figure 11a). However, there are also regions of significant mismatch along the east African coast and in South Africa. The correlation coefficients of the TPW are always very high (close to 1) in all areas where data are available (Figure 11b).

[37] TES data covers wider regions, particularly over oceans (Figure 11c and 11d). The correlation coefficients for δD vary for different locations. They have rather low values over the tropics, but higher values toward higher latitude (poleward of 20°) because weather patterns are more controlled by large-scale dynamics than local parameterized processes in the higher latitudes (consistent with the work of *Yoshimura et al.* [2003, 2008] and *Risi et al.* [2010b]). The same figure for humidity shows generally larger correlation coefficients, but a similar tendency of low correlations in the inner tropics is observable. This is due to the generally small seasonality in these tropical bands.

[38] Figure 12 shows the slopes of linearly regressed relationships between the model and the satellite data. As partly known in the Figures 9 and 10, for δD, the slope is mostly greater than 1 in SCIAMACHY (Figures 12a) and mostly smaller than 1 in TES (Figure 12c). Interestingly, slopes for humidity are less than 1 for both cases in the large part (Figures 12b and 12d), but in average, similar to correlations, these numbers are closer to 1 than those of δD. From this Figure 12, it is implicated that there is some potential to give some additional constraint to the model when SCIAMACHY data is assimilated. In case of TES, there could be potential over subtropical regions (20° ~ 40°, where slope is more than 0.8) in both hemispheres, but limited impact could be expected particularly over tropical oceans where the slope is very small (less than 0.4).

4. Summary and Conclusions

[39] In preparation for data assimilation of water isotope information, we have performed an intensive comparison of an isotope-incorporated AGCM with vapor isotopologue ratio observation data by two satellite sensors. A global IsoGSM simulation nudged toward the reanalysis dynamical field, atmospheric column data from SCIAMACHY on Envisat, and midtropospheric (800 to 500 hPa) data from TES on Aura were used. The model reproduced the geographical variability of the mean climatological δD of the total atmospheric column and of the midtroposphere quite well. There is, however, a clear underestimation of the latitudinal gradient (higher δD in the tropics and lower δD in midlatitudes) compared to the SCIAMACHY data, whereas

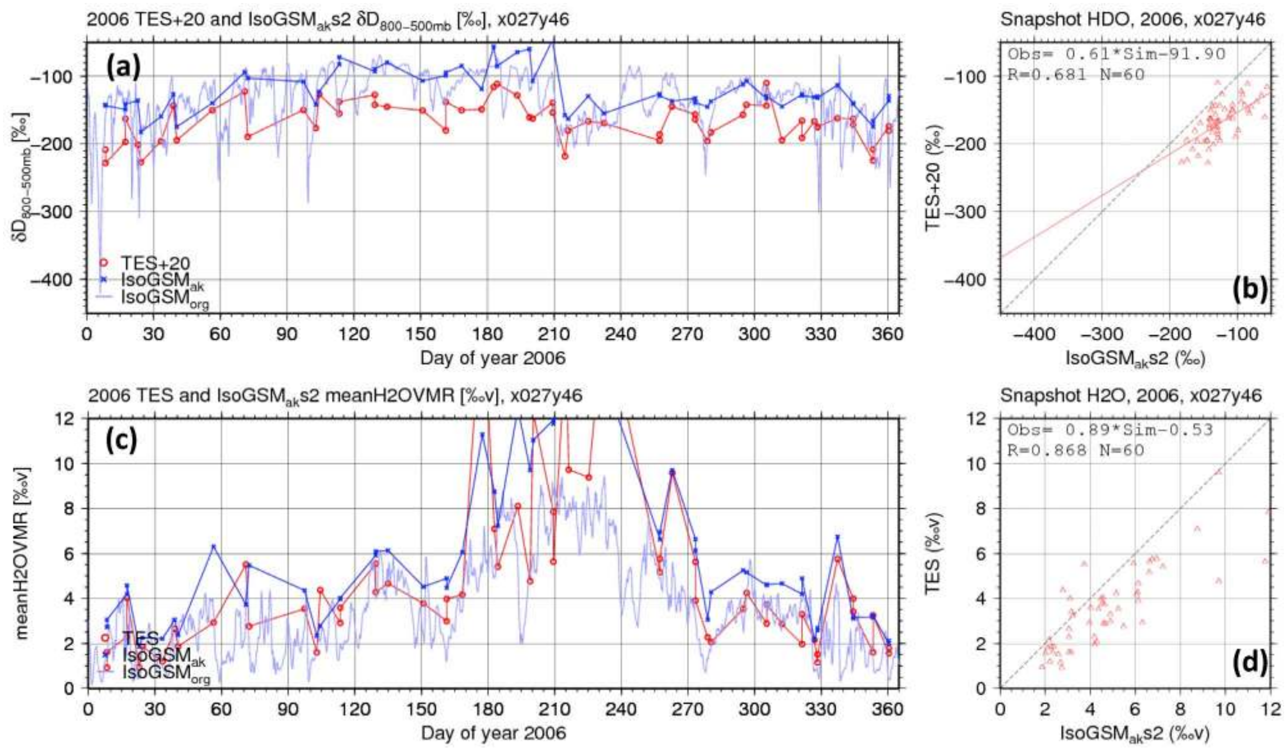

Figure 10. Similar to Figure 9 but for TES midtropospheric data at 67.5°E and 25°N. Unlike Figure 9, there is no small red dot and each red circle represents a single measurement by TES. The 6 hourly IsoGSM simulation results without averaging kernels application are shown by sky blue lines.

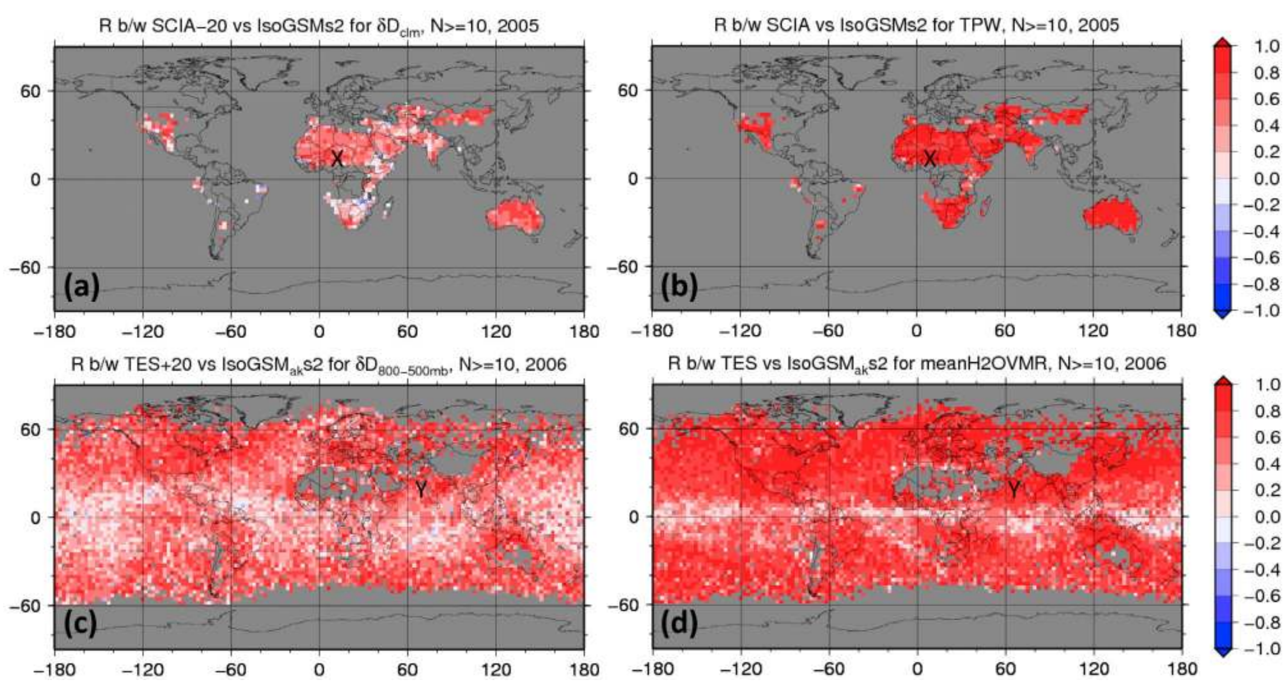

Figure 11. Global distribution maps of correlation coefficients between the time series of the SCIAMACHY or TES observations and the IsoGSM E10 simulation; (a) SCIAMACHY atmospheric column δD, (b) SCIAMACHY total precipitable water, (c) TES midtropospheric δD, and (d) TES midtropospheric volume mixing ratio. Gray areas indicate that there are not enough number of data for valid regression. “X” and “Y” indicate the approximate locations of the grids for Figures 9 and 10, respectively.

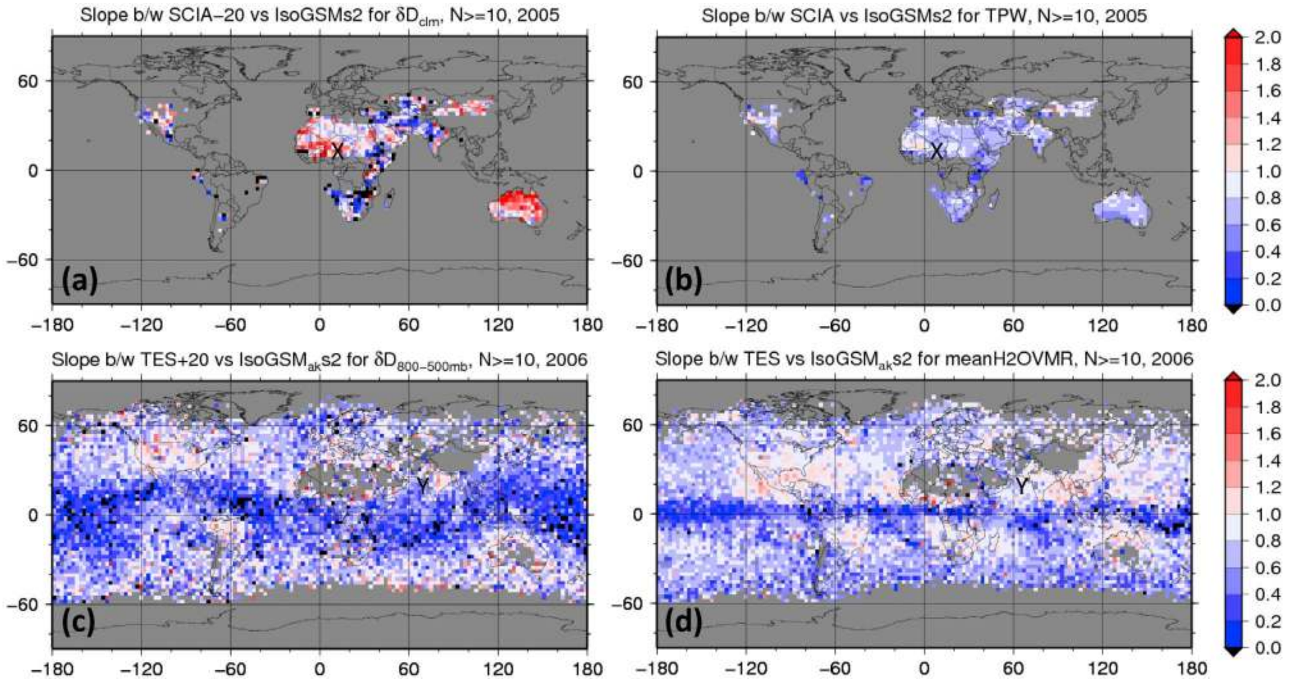

Figure 12. Similar to Figure 11 but for slope of the linearly regressed relationship.

there is generally less disagreement except lower δD over the Maritime Continent compared to the TES data.

[40] It was found that the two satellite products have different relationships between the water vapor amount and its isotopologue ratio. In many ways, both satellite products are complementary (SCIAMACHY samples total column and is best over the continents whereas TES measures between 500 and 800 hPa and is most reliable over oceans). Particularly, atmospheric column mean δD, which is dominated by lower-tropospheric vapor, exhibits a closer relationship with a typical Rayleigh-type rain out process with isotopic fractionation, whereas in the midtroposphere it is more affected by a "mixing" process. This feature is not quite reproduced by the model, where the relationships between δD and the vapor are similar to each other for both the atmospheric column and the midtroposphere, i.e., both are mainly driven by the Rayleigh-type rain out process. The seasonal variations of the vapor δD were generally adequately reproduced by the model, with some exceptions in particular regions. These regions include midlatitudes in the Southern Hemisphere for atmospheric column δD and the Maritime Continent (20°S–20°N and 90°E–180°) for midtropospheric δD. The discrepancy over the Maritime Continent is likely derived from the poor representation of the isotopic behavior in convective processes, and it was slightly improved in the model run where the equilibrium fraction was reduced, which restrains the isotopic exchange between falling droplets and ambient vapor.

[41] Finally, we compared the model and the satellite data on a shorter time scale. We found that for total column δD, SCIAMACHY measurements show larger fluctuations than the model, but both data sets correlate reasonably well. On the contrary for midtropospheric δD, the model's short-term fluctuation range is larger in the mode than for TES measurement. It is clear that the data situation for future data assimilation is best for tropical and subtropical desert areas (i.e., Sahel, southern Africa, middle eastern Asia, Gobi, Australia, and southwestern United States) for total column δD, whereas the available midtropospheric δD observations cover wider regions, particularly over oceans. However, the measurement precision and sampling frequency of future instruments such as TROPOMI will provide more, and more reliable, total column isotopologue ratio observations. The same is perhaps true with the Infrared Atmospheric Sounding Interferometer (IASI) data, which has a higher temporal and spatial resolution [*Schneider and Hase*, 2011]. However, it must be noted that neither TES nor SCIAMACHY nor TROPOMI nor IASI are dedicated water isotopologue ratio instruments and this product was not an official target when these instruments were designed.

[42] This paper compared two satellite products and a model simulation on various scales in time and space. Some of the discrepancies between the model and the observations found in this study could be corrected when performing data assimilation, which may lead to significant improvement of four-dimensional analyses of water isotope ratio distribution, which in turn would provide us with information to investigate further details of atmospheric hydrologic cycles. It is of prime importance to more understand the uncertainties of the satellite data.

[43] **Acknowledgments.** A part of this research was funded by the Japan Society for the Promotion of Science (JSPS) grant 23686071. The numerical simulations were performed with computing resources at the Center for Observations and Prediction at Scripps (COMPAS) and at TeraGrid. Part of this work was also funded by the California Energy Commission Public Interest Energy Research (PIER) program, which supports the California Climate Change Center (award MGC-04-04) and NOAA (NA17RJ1231). The views expressed herein are those of the authors and

do not necessarily reflect the views of NOAA. We would like to thank J. Roads for his encouragement in the beginning of this study. The assistance of Ms. D. Boomer in refining the writing is appreciated. The authors thank all the comments from two reviewers including Matthias Schneider.

References

Abe, O., S. Agata, M. Morimoto, M. Abe, K. Yoshimura, T. Hiyama, and N. Yoshida (2009), A 6.5-year continuous record of sea surface salinity and seawater isotopic composition at Harbor of Ishigaki Island, southwest Japan, *Isotopes Environ. Health Stud.*, *45*, 247–258, doi:10.1080/10256010903083847.

Berkelhammer, M., L. Stott, K. Yoshimura, K. Johnson, and A. Sinha (2011), Synoptic and mesoscale controls on the isotopic composition of precipitation in the southwestern US, *Clim. Dyn.*, in press.

Bowen, G. J. (2008), Spatial analysis of the intra-annual variation of precipitation isotope ratios and its climatological corollaries, *J. Geophys. Res.*, *113*, D05113, doi:10.1029/2007JD009295.

Craig, H., and L. Gordon (1965), Deuterium and oxygen-18 variations in the ocean and the marine atmosphere, in *Stable Isotopes in Oceanographic Studies and Paleotemperatures*, edited by E. Tongiorgi, pp. 9–130, V. Lischi, Pisa, Italy.

Dansgaard, W. (1964), Stable isotopes in precipitation, *Tellus*, *16*, 436–468, doi:10.1111/j.2153-3490.1964.tb00181.x.

Dansgaard, W., S. J. Johnsen, J. Møller, and C. C. Langway Jr. (1969), One thousand centuries of climatic record from camp century on the Greenland ice sheet, *Science*, *166*, 377–380, doi:10.1126/science.166.3903.377.

Ehhalt, D. H. (1974), Vertical profiles of HTO, HDO and H_2O in the troposphere, *Tech. Rep. NCAR-TN/STR-100*, Natl. Cent. for Atmos. Res., Boulder, Colo.

Field, R. D., D. B. A. Jones, and D. P. Brown (2010), Effects of postcondensation exchange on the isotopic composition of water in the atmosphere, *J. Geophys. Res.*, *115*, D24305, doi:10.1029/2010JD014334.

Frankenberg, C., et al. (2009), Dynamic processes governing the isotopic composition of water vapor as observed from space and ground, *Science*, *325*, 1374–1377, doi:10.1126/science.1173791.

Galewsky, J., and J. V. Hurley (2010), An advection-condensation model for subtropical water vapor isotopic ratios, *J. Geophys. Res.*, *115*, D16116, doi:10.1029/2009JD013651.

Gedzelman, S. D., and R. Arnold (1994), Modeling the isotopic composition of precipitation, *J. Geophys. Res.*, *99*, 10,455–10,471, doi:10.1029/93JD03518.

Hoffmann, G., M. Werner, and M. Heimann (1998), The water isotope module of the ECHAM Atmospheric General Circulation Model: A study on timescales from days to several years, *J. Geophys. Res.*, *103*, 16,871–16,896, doi:10.1029/98JD00423.

Joussaume, S., R. Sadourny, and J. Jouzel (1984), A general circulation model of water isotope cycles in the atmosphere, *Nature*, *311*, 24–29, doi:10.1038/311024a0.

Jouzel, J. (1986), Isotopes in cloud physics: Multiphase and multistage condensation processes, in *Handbook of Environmental Isotope Geochemistry*, vol. 2, edited by P. Fritz and J. C. Fontes, pp. 61–112, Elsevier, New York.

Jouzel, J., G. L. Russell, R. J. Suozzo, R. D. Koster, J. W. C. White, and W. S. Broecker (1987), Simulations of HDO and H_2 ^{18}O atmospheric cycles using the NASA GISS general circulation model: The seasonal cycle for present-day conditions, *J. Geophys. Res.*, *92*, 14,739–14,760, doi:10.1029/JD092iD12p14739.

Kanamitsu, M., W. Ebisuzaki, J. Woolen, J. Potter, and M. Fiorino (2002), NCEP-DOE AMIP-II Reanalysis (R-2), *Bull. Am. Meteorol. Soc.*, *83*, 1631–1643, doi:10.1175/BAMS-83-11-1631.

Kurita, N., N. Yoshida, G. Inoue, and E. A. Chayanova (2004), Modern isotope climatology of Russia: A first assessment, *J. Geophys. Res.*, *109*, D03102, doi:10.1029/2003JD003404.

Lawrence, J. R., S. D. Gedzelman, D. Dexheimer, H. K. Cho, G. D. Carrie, R. Gasparini, C. R. Anderson, K. P. Bowman, and M. I. Biggerstaff (2004), Stable isotopic composition of water vapor in the tropics, *J. Geophys. Res.*, *109*, D06115, doi:10.1029/2003JD004046.

Lee, J., J. Worden, D. Noone, K. Bowman, A. Eldering, A. Legrande, J.-L. F. Li, G. Schmidt, and H. Sodemann (2011), Relating tropical ocean clouds to moist processes using water vapor isotope measurements, *Atmos. Chem. Phys.*, *11*, 741–752, doi:10.5194/acp-11-741-2011.

Lee, J.-E., and I. Fung (2008), "Amount effect" of water isotopes and quantitative analysis of post-condensation processes, *Hydrol. Processes*, *22*, 1–8, doi:10.1002/hyp.6637.

Lee, J.-E., I. Fung, D. J. DePaolo, and C. C. Henning (2007), Analysis of the global distribution of water isotopes using the NCAR atmospheric general circulation model, *J. Geophys. Res.*, *112*, D16306, doi:10.1029/2006JD007657.

Lee, J.-E., R. Pierrehumbert, A. Swann, and B. R. Lintner (2009), Sensitivity of stable water isotopic values to convective parameterization schemes, *Geophys. Res. Lett.*, *36*, L23801, doi:10.1029/2009GL040880.

Lee, X., R. Smith, and J. Williams (2006), Water vapor $^{18}O/^{16}O$ isotope ratio in surface air in New England, USA, *Tellus, Ser. B*, *58*, 293–304.

Levelt, P. F. (Ed.) (2008), Final report of TROPOMI user workshop, *Rep. RP-TROPOMI-KNMI-015*, 28 pp., R. Neth. Meteorol. Inst., De Bilt, Netherlands.

Majoube, M. (1971a), Oxygen-18 and deuterium fractionation between water and steam [in French], *J. Chim. Phys.*, *68*, 1423–1436.

Majoube, M. (1971b), Fractionation in O-18 between ice and water vapor [in French], *J. Chim. Phys.*, *68*, 625–636.

Mathieu, R., D. Pollard, J. E. Cole, J. W. C. White, R. S. Webb, and S. L. Thompson (2002), Simulation of stable water isotope variations by the GENESIS GCM for modern conditions, *J. Geophys. Res.*, *107*(D4), 4037, doi:10.1029/2001JD900255.

Noone, D., and I. Simmonds (2002), Associations between $\delta^{18}O$ of water and climate parameters in a simulation of atmospheric circulation 1979–95, *J. Clim.*, *15*, 3150–3169, doi:10.1175/1520-0442(2002)015<3150:ABOOWA>2.0.CO;2.

Noone, D., and C. Sturm (2010),Comprehensive dynamical models of global and regional water isotope distributions, in *Isoscapes: Understanding Movement, Pattern, and Process on Earth Through Isotope Mapping*, edited by J. B. West et al., pp. 195–219, Springer, New York.

Numaguti, A. (1999), Origin and recycling processes of precipitating water over the Eurasian continent: Experiments using an atmospheric general circulation model, *J. Geophys. Res.*, *104*(D2), 1957–1972, doi:10.1029/1998JD200026.

Payne, V. H., D. Noone, A. Dudhia, C. Piccolo, and R. G. Grainger (2007), Global satellite measurements of HDO and implications for understanding the transport of water vapour into the stratosphere, *Q. J. R. Meteorol. Soc.*, *133*, 1459–1471, doi:10.1002/qj.127.

Risi, C., S. Bony, and F. Vimeux (2008), Influence of convective processes on the isotopic composition ($\delta^{18}O$ and δD) of precipitation and water vapor in the tropics: 2. Physical interpretation of the amount effect, *J. Geophys. Res.*, *113*, D19306, doi:10.1029/2008JD009943.

Risi, C., S. Bony, F. Vimeux, C. Frankenberg, D. Noone, and J. Worden (2010a), Understanding the Sahelian water budget through the isotopic composition of water vapor and precipitation, *J. Geophys. Res.*, *115*, D24110, doi:10.1029/2010JD014690.

Risi, C., S. Bony, F. Vimeux, and J. Jouzel (2010b), Water-stable isotopes in the LMDZ4 general circulation model: Model evaluation for present-day and past climates and applications to climatic interpretation of tropical isotopic records, *J. Geophys. Res.*, *115*, D12118, doi:10.1029/2009JD013255.

Schmidt, G. A., G. Hoffmann, D. T. Shindell, and Y. Hu (2005), Modeling atmospheric stable water isotopes and the potential for constraining cloud processes and stratosphere-troposphere water exchange, *J. Geophys. Res.*, *110*, D21314, doi:10.1029/2005JD005790.

Schneider, M., and F. Hase (2011), Optimal estimation of tropospheric H_2O and δD with IASI/METOP, *Atmos. Chem. Phys. Discuss.*, *11*, 16,107–16,146, doi:10.5194/acpd-11-16107-2011.

Schneider, M., K. Yoshimura, F. Hase, and T. Blumenstock (2010), The ground-based FTIR network's potential for investigating the atmospheric water cycle, *Atmos. Chem. Phys.*, *10*, 3427–3442, doi:10.5194/acp-10-3427-2010.

Steinwagner, J., M. Milz, T. von Clarmann, N. Glatthor, U. Grabowski, M. Höpfner, G. P. Stiller, and T. Röckmann (2007), HDO measurement with MIPAS, *Atmos. Chem. Phys.*, *7*, 2601–2615, doi:10.5194/acp-7-2601-2007.

Steinwagner, J., S. Fueglistaler, G. Stiller, T. von Clarmann, M. Kiefer, P. P. Borsboom, A. van Delden, and T. Röckmann (2010), Tropical dehydration processes constrained by the seasonality of stratospheric deuterated water, *Nat. Geosci.*, *3*, 262–266, doi:10.1038/ngeo822.

Tindall, J. C., P. J. Valdes, and L. C. Sime (2009), Stable water isotopes in HadCM3: Isotopic signature of El Niño–Southern Oscillation and the tropical amount effect, *J. Geophys. Res.*, *114*, D04111, doi:10.1029/2008JD010825.

Uemura, R., Y. Matsui, K. Yoshimura, H. Motoyama, N. Yoshida (2008), Evidence of deuterium excess in water vapor as an indicator of ocean surface conditions, *J. Geophys. Res.*, *113*, D19114, doi:10.1029/2008JD010209.

Webster, C. R., and A. J. Heymsfield (2003), Water isotope ratios D/H, $^{18}O/^{16}O$, 17O/^{16}O in and out of clouds map dehydration pathways, *Science*, *302*, 1742–1745, doi:10.1126/science.1089496.

Welker, J. M. (2000), Isotopic ($\delta^{18}O$) characteristics of weekly precipitation collected across the USA: An initial analysis with application to water source studies, *Hydrol. Processes*, *14*, 1449–1464, doi:10.1002/1099-1085(20000615)14:8<1449::AID-HYP993>3.0.CO;2-7.

Welp, L. R., X. Lee, K. Kim, T. J. Griffis, K. A. Billmark, and J. M. Baker (2008), δ^{18}O of water vapour, evapotranspiration and the sites of leaf water evaporation in a soybean canopy, *Plant Cell Environ.*, *31*, 1214–1228, doi:10.1111/j.1365-3040.2008.01826.x.

Worden, J., et al. (2006), Tropospheric Emission Spectrometer observations of the tropospheric HDO/H_2O ratio: Estimation approach and characterization, *J. Geophys. Res.*, *111*, D16309, doi:10.1029/2005JD006606.

Worden, J, D. Noone, and K. Bowman (2007), Importance of rain evaporation and continental convection in the tropical water cycle, *Nature*, *445*, 528–532, doi:10.1038/nature05508.

Worden, J., D. Noone, J. Galewsky, A. Bailey, K. Bowman, D. Brown, J. Hurley, S. Kulawik, J. Lee, and M. Strong (2011), Estimate of bias in Aura TES HDO/H_2O profiles from comparison of TES and in situ HDO/H_2O measurements at the Mauna Loa observatory, *Atmos. Chem. Phys.*, *11*, 4491–4503, doi:10.5194/acp-11-4491-2011.

Yoshimura, K., and M. Kanamitsu (2008), Dynamical global downscaling of global reanalysis, *Mon. Weather Rev.*, *136*, 2983–2998, doi:10.1175/2008MWR2281.1.

Yoshimura, K., T. Oki, N. Ohte, and S. Kanae (2003), A quantitative analysis of short-term ^{18}O variability with a Rayleigh-type isotope circulation model, *J. Geophys. Res.*, *108*(D20), 4647, doi:10.1029/2003JD003477.

Yoshimura, K., T. Oki, and K. Ichiyanagi (2004), Evaluation of two-dimensional atmospheric water circulation fields in reanalyses by using precipitation isotopes databases, *J. Geophys. Res.*, *109*, D20109, doi:10.1029/2004JD004764.

Yoshimura, K., M. Kanamitsu, D. Noone, and T. Oki (2008), Historical isotope simulation using Reanalysis atmospheric data, *J. Geophys. Res.*, *113*, D19108, doi:10.1029/2008JD010074.

Yoshimura, K., M. Kanamitsu, and M. Dettinger (2010), Regional downscaling for stable water isotopes: A case study of an atmospheric river event, *J. Geophys. Res.*, *115*, D18114, doi:10.1029/2010JD014032.

Zakharov, V. I., R. Imasu, K. G. Gribanov, G. Hoffmann, and J. Jouzel (2004), Latitudinal distribution of the deuterium to hydrogen ratio in the atmosphere water vapor retrieved from IMG/ADEOS data, *Geophys. Res. Lett.*, *31*, L12104, doi:10.1029/2004GL019433.

C. Frankenberg and J. Worden, Jet Propulsion Laboratory, NASA, 4800 Oak Grove Dr., Pasadena, CA 91109, USA.

M. Kanamitsu, Scripps Institution of Oceanography, University of California, San Diego, 8605 La Jolla Shores Dr., La Jolla, CA 92093-0224, USA.

J. Lee, Korea Polar Research Institute, Incheon 406-840, South Korea.

T. Röckmann, Institute for Marine and Atmospheric Research Utrecht, Princetonplein 5, PO Box 80000, Utrecht NL-3508, Netherlands.

K. Yoshimura, Atmosphere and Ocean Research Institute, University of Tokyo, 5-1-5 Kashiwanoha, Kashiwa, Chiba 277-8568, Japan. (kei@aori.u-tokyo.ac.jp)